ACS Photonics

Article

pubs.acs.org/journal/apchd5

Graphene–Bi_2Te_3 Heterostructure as Saturable Absorber for Short Pulse Generation

Haoran Mu,[†,§] Zhiteng Wang,[‡,§] Jian Yuan,[†,§] Si Xiao,[∥] Caiyun Chen,[†] Yu Chen,[‡] Yao Chen,[†] Jingchao Song,[⊥] Yusheng Wang,[†] Yunzhou Xue,[†] Han Zhang,*[,‡] and Qiaoliang Bao*[,†,⊥]

[†]Institute of Functional Nano and Soft Materials (FUNSOM), Jiangsu Key Laboratory for Carbon-Based Functional Materials and Devices, and Collaborative Innovation Center of Suzhou Nano Science and Technology, Soochow University, Suzhou 215123, People's Republic of China

[‡]SZU-NUS Collaborative Innovation Center for Optoelectronic Science and Technology, and Key Laboratory of Optoelectronic Devices and Systems of Ministry of Education and Guangdong Province, College of Optoelectronic Engineering, Shenzhen University, Shenzhen 518060, People's Republic of China

[∥]Institute of Super-Microstructure and Ultrafast Process in Advanced Materials, School of Physics and Electronics, Hunan Key Laboratory for Super-Microstructure and Ultrafast Process, Central South University, Changsha 410083, People's Republic of China

[⊥]Department of Materials Science and Engineering, Monash University, Clayton, VIC 3800, Australia

Supporting Information

ABSTRACT: Rapid progresses have been achieved in the photonic applications of two-dimensional materials such as graphene, transition metal dichalcogenides, and topological insulators. The strong light–matter interactions and large optical nonlinearities in these atomically thin layered materials make them promising saturable absorbers for pulsed laser applications. Either Q-switching or mode-locking pulses with particular output characteristics can be achieved by using different saturable absorbers. However, it remains still very challenging to produce saturable absorbers with tunable optical properties, in particular, carrier dynamics, saturation intensity as well as modulation depth, to suit for self-starting, high energy or ultrafast pulse laser generation. Here we report a new type of saturable absorber which is a van der Waals heterostructure consisting of graphene and Bi_2Te_3. The synergetic integration of these two materials by epitaxial growth affords tunable optical properties, that is, both the photocarrier dynamics and the nonlinear optical modulation are variable by tuning the coverage of Bi_2Te_3 on graphene. We further fabricated graphene–Bi_2Te_3 saturable absorbers and incorporated them into a 1.5 μm fiber laser to demonstrate both Q-switching and mode-locking pulse generation. This work provides a new insight for tailoring two-dimensional heterostructures so as to develop desired photonic applications.

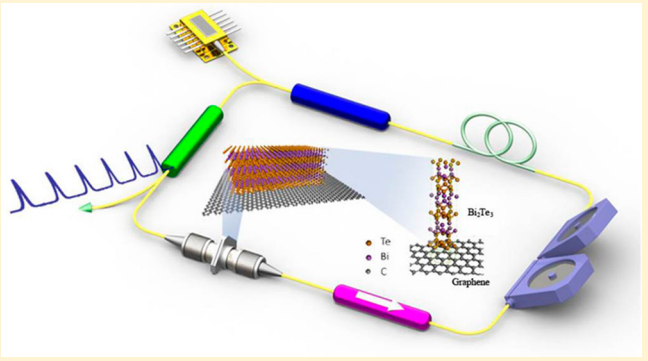

KEYWORDS: *heterostructure, graphene, saturable absorber, Q-switching, mode-locking*

Graphene has been demonstrated to be a new and effective saturable absorber for the pulsed laser.[1] There are two important characteristics for graphene photonics: the first one is its inherent ultrawide spectral range due to the linear dispersion near the Dirac point, which enables the occurrence of saturable absorption over a very broad operation wavelength range; the second one is its ultrafast recovery time (intraband relaxation time <150 fs), which affords the capability to generate shorter pulse than other saturable absorption materials.[2] These properties are not observed in conventional semiconductor saturable absorber mirror (SESAM)[3] and carbon nanotube (CNT) based saturable absorbers.[4] Till now, graphene has been used for the generation of Q-switched and mode-locked pulses in fiber lasers,[1,5−9] solid lasers,[10−12] and waveguide lasers,[13] in which the working wavelength is covered from 800 nm[11] to 3 μm.[7] Nevertheless, there are some shortcomings for graphene-based SAs even though intensive efforts have been made. In particular, the absolute optical modulation depth of monolayer graphene is very low (typically around 1%) due to the relatively low absorption strength of one atomic layer.[14] Despite that the increase in the number of graphene layers can enhance the modulation depth, unwanted nonsaturable losses will also rise, which might be not desirable for practical laser applications.

Inspired by the progress in graphene-based saturable absorber, many other grephene-like two-dimensional (2D) nanomaterials, such as topological insulators (TIs, for example,

Received: December 5, 2014
Published: June 8, 2015

DOI: 10.1021/acsphotonics.5b00193
ACS Photonics 2015, 2, 832−841

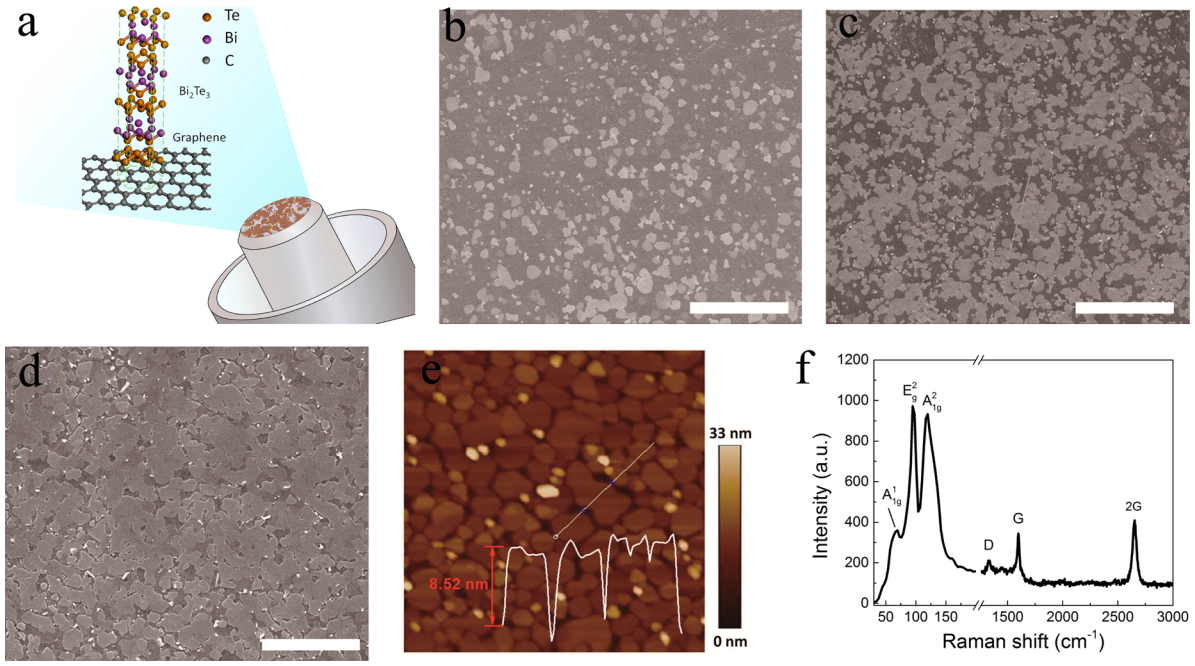

Figure 1. Material characterizations of graphene–Bi_2Te_3 heterostructure. (a) Schematic of graphene–Bi_2Te_3 heterostructure on the end-facet of fiber connector. (b–d) SEM images with 15, 65, and 85% coverage of Bi_2Te_3, respectively. The scale bars are all 10 μm. (e) AFM image of the Bi_2Te_3 nanoplatelets on a SiO_2 substrate. (f) Raman spectrum of the graphene–Bi_2Te_3 heterostructure.

Bi_2Se_3,[15,16] Bi_2Te_3,[17–20] and Sb_2Te_3[21,22]), and transition metal dichalcogenides (TMDs, for example, MoS_2[23–25]), have been demonstrated to be new candidates for saturable absorbers that have similar applications in short pulse generation. Among those new saturable absorption materials, TIs have a very high modulation depth (~70% at the wavelength of 1570 nm),[26] but the transient carrier dynamics, specifically, the relaxation time of intraband excitation is quite long (>500 fs) according to theoretical and experimental investigations, indicating that TIs are relatively slower SAs in comparison with graphene.[27–29] By choosing a suitable saturable absorber, either Q-switching or mode-locking pulses with particular output characteristics can be achieved. In a recent report,[9] the modulation depth of graphene can also be adjusted through an additional modulating light, and mode-locking pulses can be generated with tunable pulse duration. However, it is still very challenging to make saturable absorbers with controllable carrier dynamics as well as modulation depth to achieve different laser operation states. Here we provided a material design approach to produce saturable absorbers with controllable optical properties.

In the paper, we controllably grow graphene–Bi_2Te_3 heterostructures and systematically investigated the carrier dynamics as well as the corresponding nonlinear optical properties. Our work suggests that the exciton relaxation time of graphene–Bi_2Te_3 heterostructure is tunable depending on the coverage of Bi_2Te_3, and their modulation depth is also tunable and much higher than monolayer graphene due to larger absorption from Bi_2Te_3 nanocrystals. We further fabricated graphene–Bi_2Te_3 SAs and integrated them into a 1.5 μm fiber laser to realize both Q-switching and mode-locking pulse generation.

RESULTS AND DISCUSSION

Material Characterizations. The graphene–Bi_2Te_3 heterostructure materials were produced by two-step chemical vapor deposition (CVD) in which monolayer graphene thin film was grown on copper substrate, and subsequently, Bi_2Te_3 nanoplatelets were deposited on graphene substrate. Unlike the general method, which just mechanically overlaps Bi_2Te_3 with graphene, in our approach thin nanocrystals of Bi_2Te_3 are directly grown on graphene film and can form van der Waals interactions between these two materials. Due to the similar hexagonal crystal structure, small lattice mismatch (~2.7%), and similar thermal expansion coefficient, the heterostructure consisting of graphene and Bi_2Te_3 has a well-defined interface facilitating the transfer of photoexcited carriers.[30–32] Using a wet-chemistry transfer technique similar to that used for CVD graphene, the graphene–Bi_2Te_3 heterostructure thin film can be easily lifted off and transferred onto other substrates. Here the sample was transferred onto the cross-section of FC/PC fiber connector (shown in Figure 1a) and then sandwiched between two fiber connectors, which is called "sandwiched structure". This combined structure can be easily integrated into fiber laser cavity as a saturable absorber device.

By changing the Ar gas flow and temperature during the epitaxial growth of Bi_2Te_3, we are able to produce graphene–Bi_2Te_3 heterostructure membranes with different coverage but the same thickness of Bi_2Te_3 layer. Three samples that have 15, 65, and 85% coverage of Bi_2Te_3 are shown in Figure 1b–d, respectively. Many nonregular shape Bi_2Te_3 nanoplatelets are found on the surface of 15% coverage sample (Figure 1b), and some of them are triangle and hexagonal, indicating single crystal nature. While the coverage is increased, those Bi_2Te_3 nanoplatelets become bigger and merge together to form a nearly continuous thin film (Figure 1d). Atomic force microscopy is further performed to characterize the morphology and thickness of graphene–Bi_2Te_3 heterostructure membrane, as shown in Figure 1e. It is found that even in the sample with very high coverage the Bi_2Te_3 nanoplatelets are still quite thin (about 8.5 nm thick).

Figure 1f shows a typical Raman spectrum at 633 nm laser excitation. The Raman peaks of graphene locates at high

DOI: 10.1021/acsphotonics.5b00193
ACS Photonics 2015, 2, 832–841

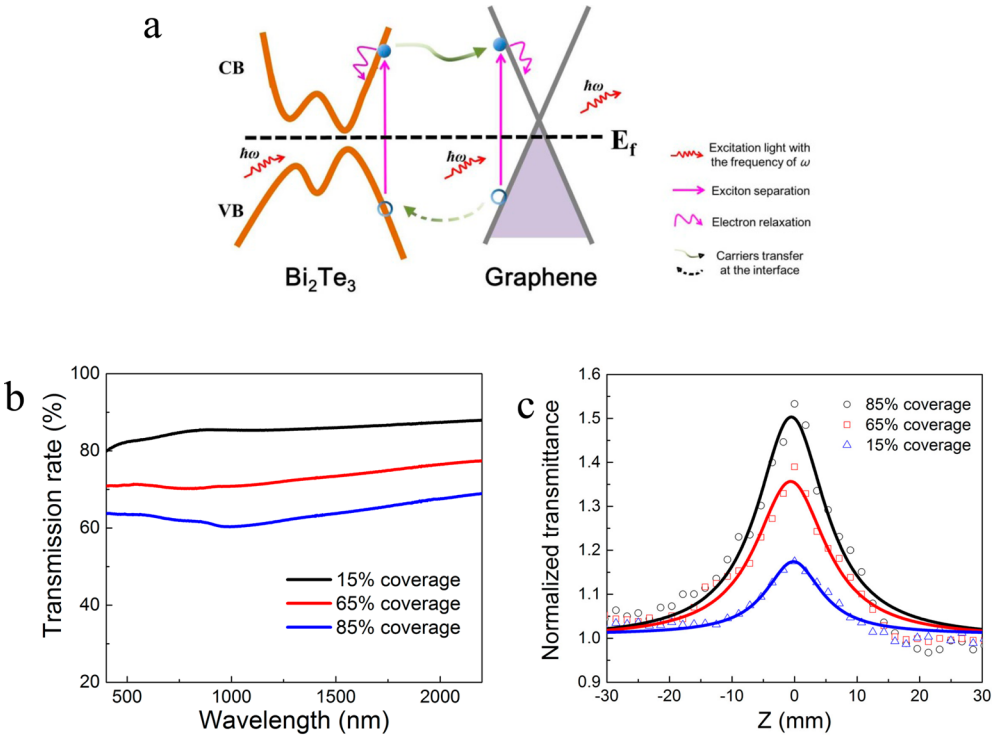

d

Bi_2Te_3 coverage	Linear transmission rate	Normalized modulation depth	Absolute modulation depth
15%	86.1%	14.7%	12.6%
65%	72.2%	34.6%	24.9%
85%	64.1%	50.1%	32.05%

Figure 2. Optical characterizations of graphene–Bi_2Te_3 heterostructure. (a) Schematic diagram showing the optical transitions in graphene–Bi_2Te_3 heterostructure. (b) UV–visible near-infrared absorption spectrum of graphene and graphene–Bi_2Te_3 heterostructure. (c) Saturable absorption data measured by an open-aperture Z-scan setup. (d) The modulation depths of graphene–Bi_2Te_3 heterostructure samples with different Bi_2Te_3 coverage.

frequency range from 1200 to 3000 cm^{-1}, while the Raman peaks of Bi_2Te_3 nanoplatelets is at the lower frequency range from 30 to 200 cm^{-1}. The two characteristic peaks 1598 (G band) and 2652 cm^{-1} (2D band) correspond to the stretching of the C–C bond and a second-order two-phonon process in sp^2 carbon hybridization, respectively. The 2D band is higher than G band, indicating that it is monolayer graphene. Compared to that of pure graphene, the G peak and 2D peak have obvious shifts (see Figure S1), which suggests the formation of heterostructure as well as interlayer interaction between graphene and Bi_2Te_3.[33] The relatively weak D band peak at 1350 cm^{-1} suggests that the graphene film is of high quality. Three characteristic peaks of Bi_2Te_3 were observed at 69.5, 94.6, and 119.7 cm^{-1}, which are consistent with the A1 1g, E2 g, and A2 1g vibrational modes of Bi_2Te_3 crystal, respectively. The coexistence of these peaks is the direct evidence of the successful formation of graphene–Bi_2Te_3 heterostructure.

Energy Structure. An energy diagram is proposed in Figure 2a to illustrate the optical excitation of carriers as well as the possible transfer process in graphene–Bi_2Te_3 heterostructure. Graphene has linear energy dispersion without bandgap, while Bi_2Te_3 has a small bandgap of about 0.165 eV for bulk state and possibly a Dirac-type surface states (binding energy of Dirac point is 0.34 eV). According to previous reports, as-grown graphene is slightly *p*-doped due to the doping effect of substrates, defects, water molecules, and oxygen in air,[34] while Bi_2Te_3 is normally *n*-doped due to Te vacancies.[35,36] Meanwhile, the work function of Bi_2Te_3 (~5.3 eV)[37,38] is higher than graphene (~4.6 eV).[39] As a result, a heterojunction similar to metal–semiconductor contact forms at the interface of graphene and Bi_2Te_3 due to the electron transfer from graphene to Bi_2Te_3. Based on this special energy structure, we are able to predict a few optical properties, that is, the heterojunction materials should have a broadband absorption characteristics from visible to infrared due to zero bandgap in

DOI: 10.1021/acsphotonics.5b00193
ACS Photonics 2015, 2, 832–841

graphene and small bandgap in Bi_2Te_3. We can also expect to see the modification of carrier dynamics in this heterostructure because the appearance of graphene provides a fast channel for the photoexcited carriers to relax, that is, the photoexcited carriers in Bi_2Te_3 will be injected into graphene and become a "Dirac Fermions" due to the band bending caused by interlayer interactions. The direct consequence is that the carrier relaxation will become faster in graphene−Bi_2Te_3 heterostructure in comparison to that in pure Bi_2Te_3. In addition, the optical absorption strength can be greatly increased by Bi_2Te_3, which could benefit to stronger optical nonlinearity and lead to larger modulation depth. These assumptions will be verified in the following section.

Optical Properties Characterization. Figure 2b shows the linear optical transmission spectra of graphene−Bi_2Te_3 heterostructure thin films. Here we choose three samples with 15, 65, and 85% coverage of Bi_2Te_3. Their transmission rate at the wavelength of 1550 nm is 86.1, 72.2, and 64.1%, respectively. The heterostructure shows a remarkably enhanced light absorption over a wide range of wavelengths due to the strong absorption of Bi_2Te_3. Furthermore, inheriting the linear optical properties of pure graphene and pure Bi_2Te_3, the graphene−Bi_2Te_3 heterostructure sample also has a relatively flat absorption curve in the visible to near-infrared wavelength range, which is desired for the broadband optical applications.

The nonlinear response of graphene−Bi_2Te_3 samples with different Bi_2Te_3 coverage is studied by the open aperture Z-scan measurement technique, and the corresponding normalized Z-scan curves are shown in Figure 2c. It is found that all the traces have a sharp and narrow peak located at the beam focus, showing the feature of optical saturable absorption (that is, optical absorbance decreases with the increase of the incident optical power but reaches at a constant value once the optical power exceeds a threshold). We interestingly note that while the coverage of Bi_2Te_3 is increased from 15 to 85%, the normalized modulation depth increases from 14.7 to 50.1%, indicating a new strategy to tune the nonlinear response of heterostructure materials by controlling the coverage. According to previous Z-scan measurements,[26,40] the normalized modulation depth of graphene and Bi_2Te_3 are 4 and 70%, respectively. The rational design of these two 2D materials achieve a tunable and compromised modulation depth, which affords particular photonic applications, such as laser mode-locking to generate pulses, in which particular modulation strength by the saturable absorber is needed.

Combined the linear transmission rate with the normalized modulation depth at the wavelength of 1550 nm, we can get the absolute modulation depth of each samples. The tunable range of absolute modulation depth is from 12.6 to 32.05%, which is far higher than that of graphene (~1% per layer). The graphene−Bi_2Te_3 heterostructure should be a promised saturable absorption material.

Carrier Dynamics. The carrier dynamic of a saturable absorber plays an important role to determine how short a pulse can be produced in passively mode-locked laser.[41] In view of the nonlinearities in time domain, the nonlinear optical response should be described by the interplay between intraband and interband dynamics. As we know, the carrier relaxation time in graphene can be described by a biexponentially decaying function, $\Delta T(t)/T = A_1 \exp(-t/\tau_1) + A_2 \exp(-t/\tau_2)$, where those two components (τ_1 and τ_2) of decay time correspond to the carrier−carrier intraband collision and interband recombination, respectively.[42] Graphene is normally considered as a fast saturable absorber because its intraband electron relaxation happens within a very short time ($\tau_1 \approx 100$ fs).[8] Its interband electron relaxation time is measured to be ~1.5 ps.[2] The carrier dynamics of Bi_2Te_3 has been measured by time-resolved angle-resolved photoemission spectroscopy (TrARPES).[27,28] Its intraband and interband relaxation times are found to be more than 500 fs and 5 ps, respectively.[27] We carried out pump−probe experiments to investigate the carrier dynamics of three heterostructure samples with different coverage of Bi_2Te_3, as discussed above. The experimental results are shown in Figures 3 and S2. After fitting the experimental data by the exponentially decaying

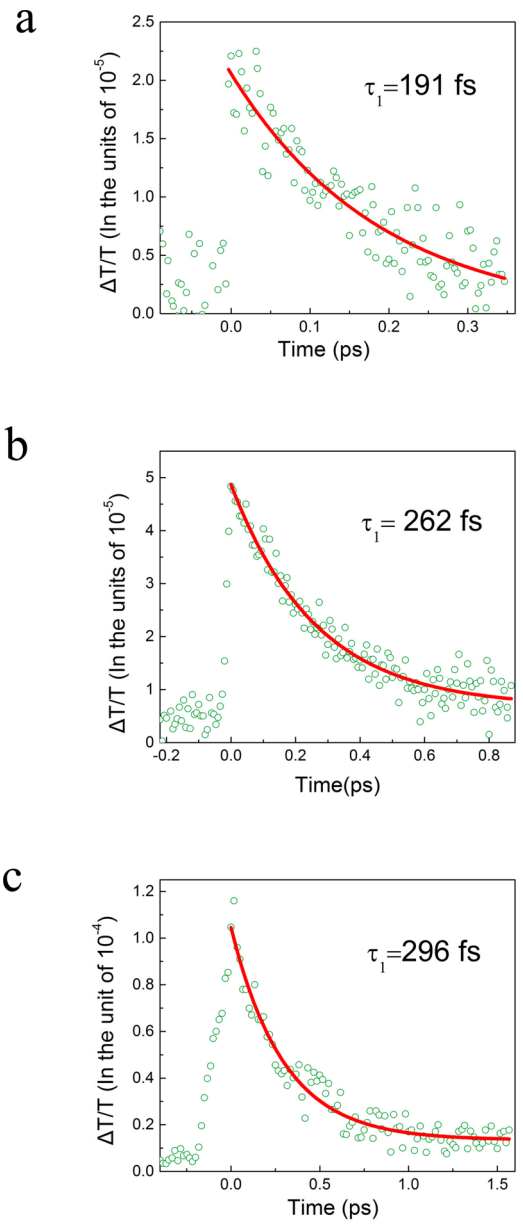

Figure 3. Transient absorption dynamics of graphene−Bi_2Te_3 heterostructure samples pumped and probed at the wavelength of 1550 nm. The open green dots are experimental data and the red curves are analytically fit to the data using exponentials with a time constant τ. (a) The sample with 15% coverage of Bi_2Te_3. (b) The sample with 65% coverage of Bi_2Te_3. (c) The sample with 85% coverage of Bi_2Te_3.

DOI: 10.1021/acsphotonics.5b00193
ACS Photonics 2015, 2, 832−841

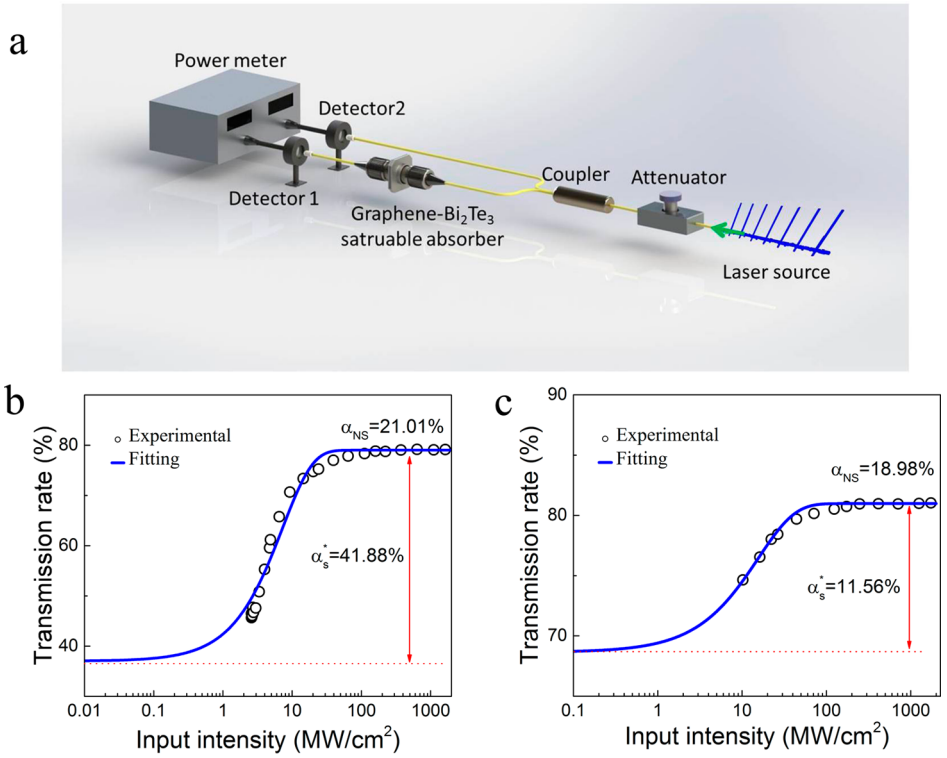

Figure 4. Saturable absorption properties of fiber-coupled graphene−Bi_2Te_3 saturable absorbers measured by twin-detector measurement technique. (a) Schematic diagram of the twin-detector measurement experimental setup. (b) Nonlinear transmission curve of a graphene−Bi_2Te_3 saturable absorber with 85% coverage of Bi_2Te_3. (c) Nonlinear transmission curve of a graphene−Bi_2Te_3 saturable absorber with 15% coverage of Bi_2Te_3.

function, it is interesting to find that the intraband relaxation constant (τ_1) is tunable, that is, τ_1 is calculated to be 191, 262, and 296 fs for the samples with 15, 65, and 85% coverage of Bi_2Te_3, respectively. The interband electron relaxation times (τ_2) of these three samples are found to be a few picoseconds (see Figure S2), which are longer than that of pure graphene. Considering that graphene is a fast saturable absorber and Bi_2Te_3 is a slower one, the formation of graphene−Bi_2Te_3 heterostructure speeds up the carrier dynamics in Bi_2Te_3 due to fast charge transfer and relaxation channel in graphene.[43] On the other hand, the interaction with Bi_2Te_3 also slows down the carrier dynamics in graphene due to additional collisions of carriers injected from Bi_2Te_3. Last, one of the important deliveries of this work is that saturable absorbers with tunable carrier dynamics are achievable via the engineering of two 2D materials. This will greatly enrich the potential photonic applications of 2D materials, including pulse laser generation and photodetection, as well as solar energy harvesting.

In-Line Saturable Absorption Measurements. In order to evaluate the modulation depth as well as the nonsaturable absorption loss of our samples, we performed in-line saturable absorption measurements on graphene-Bi_2Te_3 heterostructure samples with 15 and 85% Bi_2Te_3 coverage. The experimental setup with balanced twin-detector is shown in Figure 4a. The optical source is a passively mode-locked fiber laser with repetition rate of 8.93 MHz, central wavelength range of 1560 nm, pulse width of 1.98 ps, and output power up to 20 mW. By continuously adjusting the input power, we could record the optical transmittance under different input intensities. The saturable absorption in graphene−Bi_2Te_3 heterostructure can be fitted by

$$\alpha(I) = \frac{\alpha_S}{1 + I/I_S} + \alpha_{NS} \quad (1)$$

where α_S and α_{NS} are the saturable and nonsaturable absorption, I_S is the saturation intensity, defined as the optical intensity required in a steady state to reduce the absorption to half of its unbleached value.[1] One can deduce that graphene−Bi_2Te_3 heterostructure with 85% coverage of Bi_2Te_3 has a modulation depth of 41.88% and saturation intensity of 7.29 MW/cm^2, as shown in Figure 4b. The sample with 15% coverage of Bi_2Te_3 owns a modulation depth of 11.56% and saturation intensity of 10.95 MW/cm^2, as shown in Figure 4c. The modulation depths obtained here are close to those measured in open-aperture Z-scan measurements (i.e., 41.88 vs 32.05% and 11.56 vs 12.6%). The small discrepancy may originate from different testing conditions and fitting functions. The linear transmission rates of these two devices are 37.11 and 69.46%, respectively. And the nonsaturable losses are 21.01 and 18.98%, respectively, which are much higher than those indicated by Z-scan measurements. The reason is that extra losses such as inserting loss of fiber connector and fiber spice loss will be introduced into the measurements.

It is noteworthy that the modulation depth of heterostructure sample with 85% coverage of Bi_2Te_3 is 4× that of the sample with 15% coverage of Bi_2Te_3. It has been previously reported that comparable modulation depth can also be observed from multilayer graphene films.[1,8] However, there lacks a feasible method to produce large area multilayer graphene with controllable thickness and good uniformity. Our heterostructure materials offer us new opportunities to choose suitable saturable absorbers with desired light modulation capability as the modulation depth largely influences the output state of fiber pulse laser.

DOI: 10.1021/acsphotonics.5b00193
ACS Photonics 2015, 2, 832−841

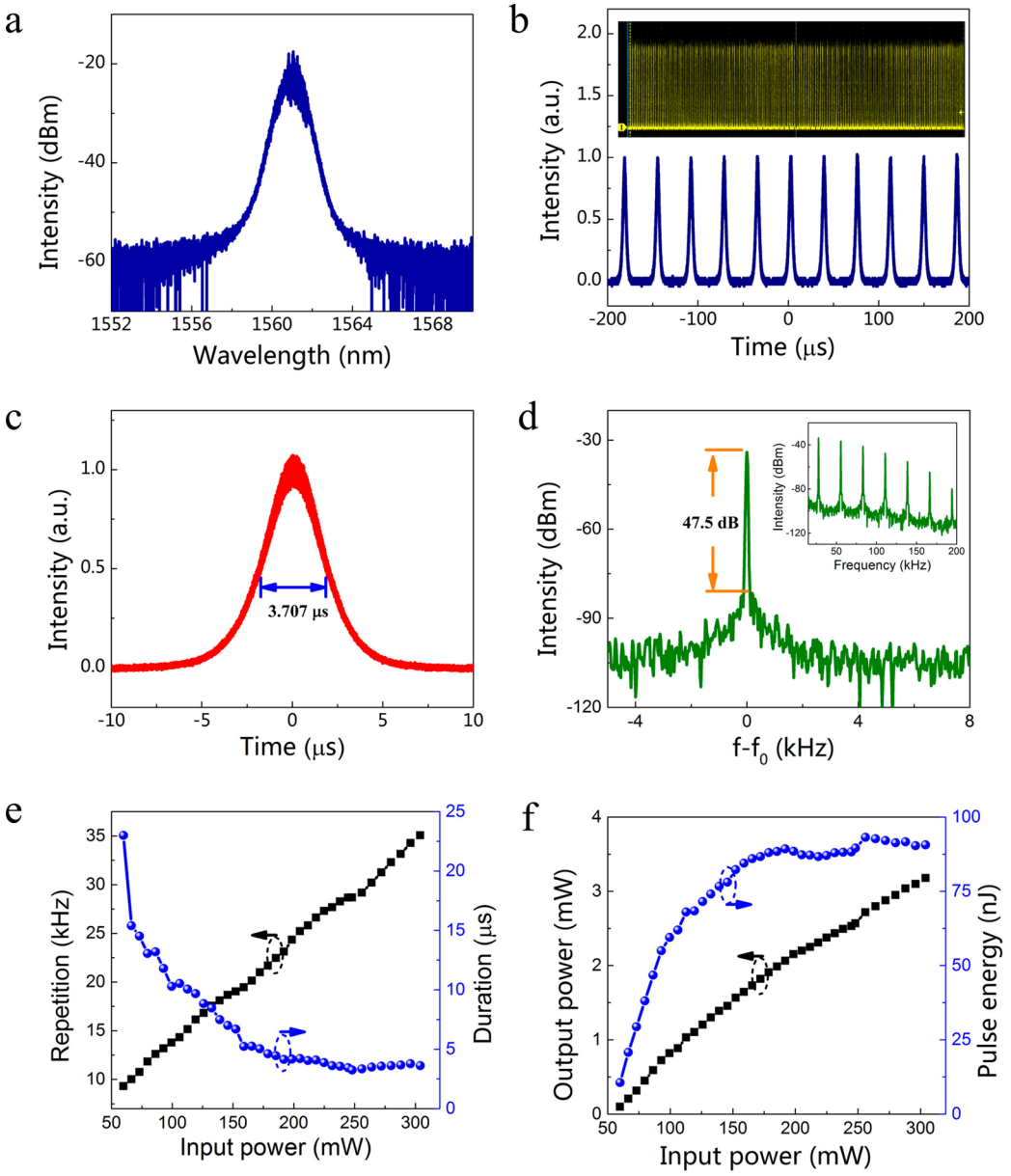

Figure 5. Typical Q-switching characteristics: (a) optical spectrum; (b). Q-switching pulse train; (c) single Q-switching pulse; (d) the radio frequency optical spectrum at the fundamental frequency and the wideband RF spectrum (inset); (e) pulse repetition rate and duration vs incident pump power; (f) output average power and pulse energy versus incident pump power.

Pulsed Laser Applications. As discussed above, we have grown graphene−Bi_2Te_3 heterostructure with controllable saturable absorption and modulation depth, as well as carrier dynamics by engineering the coverage of top layer material (i.e., Bi_2Te_3). It is intriguing to apply this new material for pulsed laser applications, either Q-switching or mode-locking, which will be elaborated hereinafter.

Laser Cavity. The configuration of the laser cavity is schematically shown in Figure 4. A piece of 3 m highly doped Erbium-doped fiber as gain medium was forward pumped by a 975 nm laser diode through a 980 nm/1550 nm wavelength division multiplexer (WDM). A polarization-independent isolator (ISO) was used to ensure the direction of light propagation. The cavity polarization state and intracavity birefringence was adjusted by a polarization controller (PC). A 10% coupler was employed to direct the output signal to oscilloscope. The single mode fiber (SMF) was added into the cavity to compress optical pulses and improve pulse quality, which is important to achieve different pulse generation regime. Two fiber-coupled saturable absorber devices (graphene−Bi_2Te_3 heterostructures with 15 and 85% coverage of Bi_2Te_3) were inserted between PC and coupler for pulse reshaping and generation.

Q-Switching. Figure 5 shows the results of a Q-switching operation state of the fiber laser using a graphene−Bi_2Te_3 heterostructure with 85% coverage of Bi_2Te_3 as saturable absorber. It was found that continuous wave operation started at a pump power of 47.4 mW and stable Q-switched operation was obtained once the pump power exceeded a threshold value of 53.3 mW. The total cavity length is about 12.5 m and a pump power of 218.3 mW is used to collect the experimental data shown in Figure 5a−d. A typical optical spectrum with a central wavelength of 1561.07 nm is depicted in Figure 5a, which gives a 3-dB spectral bandwidth of 0.52 nm. The stable

DOI: 10.1021/acsphotonics.5b00193
ACS Photonics 2015, 2, 832−841

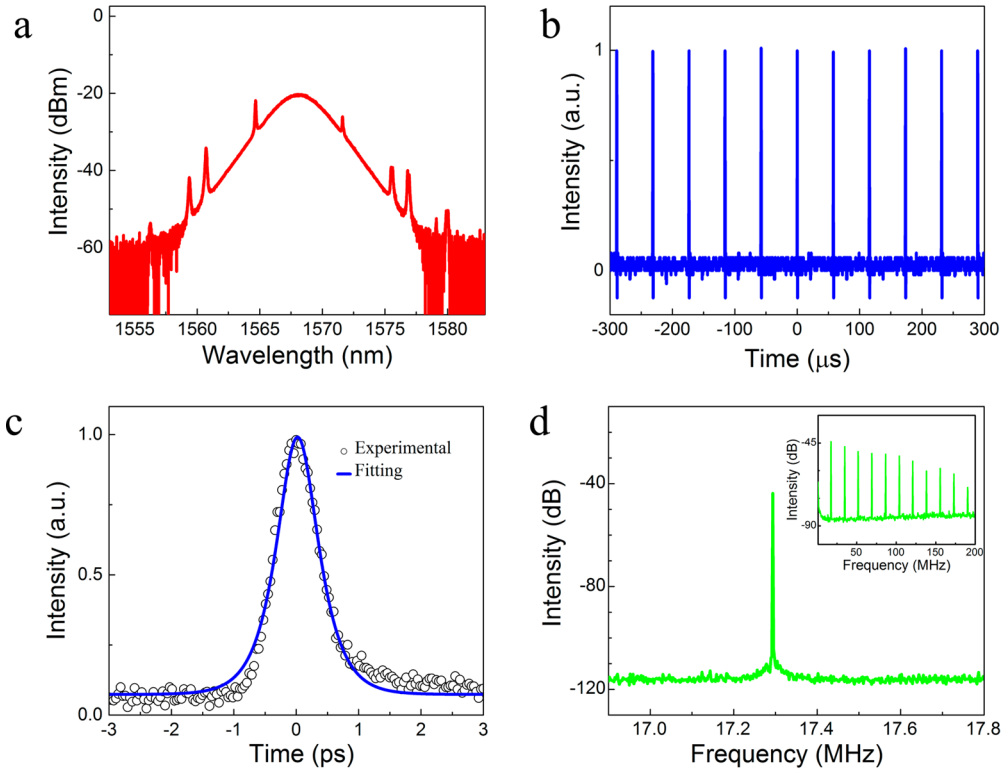

Figure 6. Typical mode-locking characteristics: (a) typical mode-locking optical spectrum; (b) mode-locking pulse train; (c) autocorrelation trace; (d) the RF optical spectrum at the fundamental frequency and the wideband RF spectrum (inset).

Q-switched pulse train has a repetition rate of 27.29 kHz, corresponding to a time interval between adjacent pulses of 36.64 μs, as shown in Figure 5b. The inset shows the pulse train in 10 ms scale, from which a nearly uniform intensity distribution without modulation was observed. All the pulses have symmetric intensity profile without any amplitude modulation (at either cavity fundamental or harmonic frequency) on each single Q-switched pulse envelope, indicating that the self-mode-locking effect had been effectively suppressed. The full width at half-maximum (fwhm) of the individual pulse is 3.707 μs, as shown in Figure 5c. To investigate the laser stability, we measured its corresponding radio frequency (RF) spectrum. As can be seen in Figure 5d, the signal-to-noise ratio (SNR) is over 47.5 dB, indicating that the Q-switched pulse operates in a relatively stable regime. Moreover, apart from the fundamental and harmonic frequency, we did not observe other frequency component in the RF spectrum with wider span as shown in the inset, further confirming high stability of the Q-switched pulse.

Figure 5e reveals the relationship between pulse duration as well as repetition rate and the pump power. With the increase of the pump power from 59.9 to 304 mW, the repetition rate increases from 9.3 to 35.07 kHz and the pulse duration decreases from 23 to 3.247 μs. Once pump power exceeds 198.5 mW, pulse duration is almost contact at around 3.5 μs, probably because of the saturation of the upper energy level. Figure 5f shows output average power and pulse energy of our Q-switched fiber laser as a function of input pump power. It is found that the average output power increases almost linearly with the input pump power and reaches a maximum at 3.197 mW, which is only limited by the maximum input pump power. By contrast, the single pulse energy increases rapidly and tends to be saturated when the pump power is further increased beyond 158.9 mW. The highest pulse energy is 93.18 nJ at a pump power of 256 mW. During the entire testing range of input power, the Q-switched pulses keep very stable, indicating a high quality and thermal stability of our graphene-Bi_2Te_3 heterojunction saturable absorber. Considering the nonlinear optical properties of this saturable absorber, we suggest that high modulation depth as well as low transmission rate blocks the self-starting of mode-locking state in a standard ring fiber laser cavity.

Soliton State Mode-Locking. By changing the length of SMF, the cavity net dispersion was tuned, and stable mode-locking can be achieved. It was found that stable mode-locking state happens at a relatively low threshold power of 40 mW using the heterostructure sample with 15% Bi_2Te_3 coverage. Figure 6 summarized the mode-locking characteristics under the pump power of 140.7 mW. The typical optical spectrum of mode-locked pulse is shown in Figure 6a. The 3 dB bandwidth is 3.4 nm and the central wavelength is around 1568.07 nm. The symmetrical sidebands are clearly observed on the spectrum, attesting to a very stable soliton state.[44] The pulse train shown in Figure 6b has a repetition rate of 17.3 MHz, which corresponds to the total cavity length of 11.56 m. Considering that the measured output power is 3.07 mW, the single pulse energy is calculated to be 0.178 nJ. The autocorrelation (AC) trace of a single soliton pulse is shown in Figure 6c, with a fwhm of 837 fs. The corresponding time-bandwidth product (TBP) is 0.34. The data is very close to the typical value of $sech^2$ pulse profile (TBP = 0.314), indicating that the soliton is very stable with little chirped.[45] To further investigate the signal-to-noise ratio, we also measured the radio frequency (RF) spectrum of the mode-locked pulses. Its fundamental peak locates at the cavity repetition rate (17.3 MHz), as shown in Figure 6d, with a signal-to-noise ratio of

DOI: 10.1021/acsphotonics.5b00193
ACS Photonics 2015, 2, 832−841

60.7 dB (10^6 contrast). The strong noise suppressing capability is associated with the ultrafast carrier dynamics (i.e., τ_1 = 191 fs) of this saturable absorber.[46] This further confirms that the soliton pulses have very high quality in terms of good stability. The inset of Figure 6d shows the wideband RF spectrum up to 200 MHz. The absence of spectral modulation in RF spectrum indicates that the laser works in a CW mode-locking regime.[3]

CONCLUSIONS

The graphene−Bi_2Te_3 heterostructure membranes with controllable optical properties were successfully produced and applied for pulsed laser generation. The formation of graphene−Bi_2Te_3 heterostructure gives a larger modulation depth than pure graphene and faster carrier dynamcis than pure Bi_2Te_3. By controlling the coverage of Bi_2Te_3 nanoplatelets, the modulation depth is tuned from 14.7 to 50.1% and the carrier relaxation time is adjusted from 191 to 296 fs. By choosing suitable G-Bi_2Te_3 materials to fabricate saturable absorber device, both typically Q-switching and mode-locking states were observed. The Q-switching pulses have a maximum output power of 3.197 mW, a highest pulse energy of 93.18 nJ, a tunable repetition rate increases from 9.3 to 35.07 kHz and a tunable pulse width from 23 to 3.247 μs. The typically mode-locking pulses have a pulse width of 837 fs with a small TBP of 0.34 which can be attributed to a stable soliton state. Our research delivers a new tunable photonics materials which may find wide applications for pulse laser generation or signal processing.

EXPERIMENTAL SECTION

A standard CVD process was used to grow graphene on 25 μm thick copper foils (Alfa Aesar, item No. 13382).[47] The graphene film was then wet-transfer onto SiO_2 substrate for further growth of Bi_2Te_3 nanoplatelets on top of it, which were produced by physical vapor deposition method in a separate tube furnace. Bi_2Te_3 powder (Alfa Aesar, purity: 99.999%) was placed in the center of the furnace (about 500 °C) as the source material for evaporation. The graphene/SiO_2 samples were placed at the region with a temperature range of 290−360 °C. Argon was used as the carrier gas to transport the Bi_2Te_3 vapor onto the graphene films. The as-produced graphene-Bi_2Te_3 heterostructure thin films were then wet-transferred onto quartz substrate for optical characterizations and cross-section of optical fiber ferrule as saturable absorber device.

The morphology of the graphene-Bi_2Te_3 heterostructure was investigated in SEM (FEI Quanta 200 FEG, acceleration voltage: 5−30 kV). The crystal morphology and thickness were characterized using a scanning probe microscopy (Bruker Multimode V). The Raman spectrum was measured on confocal micro-Raman system (Horiba Jobin-Yvon Labram HR800).

The open-aperture Z-scan measurements were performed using a femtosecond pulse laser, which was pumped by a Ti:sapphire regenerative amplifier system. The output pulses work at the central wavelength of 1550 nm with a repetition rate of 2 kHz and a pulse duration of 45 fs. The incident laser beam was focused by a lens with the focus distance of 150 mm and the beam waist is 30 μm, corresponding to peak intensity up to 13.375 GW/cm^2. 5% of the laser beam was split as the reference beam. The graphene−Bi_2Te_3 sample was mounted on a linear translation stage. The relative distance between the objective lens and the graphene−Bi_2Te_3 sample can be continuously varied by the motorized linear translation stage. A second detector was used to measure the entire laser beam intensity passing through the sample.

The transient transitivity measurements were performed using a femtosecond pulse laser with pulse duration of 45 fs and repetition rate of 2 kHz. Both the pump light and the probe light are at 1550 nm. The pump incident intensity is 0.8235 GW/cm^2 and the intensity ratio of the pump to the probe was kept at least 20:1. Any coherent artifact on the transient signal was eliminated by using the cross-polarized configuration. It has been examined that the probe beam alone could not cause any nonlinear effect in our experiments.

The fiber laser cavity consists of a piece of 3 m Erbium-doped fiber (LIEKKI Er-16/125), WDM, ISO, PC, coupler, SMF with GVD of −23 ps^2 km^{-1}, and a graphene−Bi_2Te_3 saturable absorber device. The output frequency-domain characteristics and the time-domain profile characteristics were simultaneously monitored by an optical spectrum analyzer (YOKOGAWA AQ6370C), a 1 GHz oscilloscope (Tektronix MDO3104) integrated with the RF spectrum analysis function (bandwidth: 3 GHz) and a second harmonic generation autocorrelator (FR-103MN).

ASSOCIATED CONTENT

Supporting Information

Additional supporting figures. The Supporting Information is available free of charge on the ACS Publications website at DOI: 10.1021/acsphotonics.5b00193.

AUTHOR INFORMATION

Corresponding Authors

*E-mail: hzhang@szu.edu.cn.
*E-mail: qlbao@suda.edu.cn.

Author Contributions

§These authors contributed equally to this work (H.M., Z.W., and J.Y.).

Notes

The authors declare no competing financial interest.

ACKNOWLEDGMENTS

We acknowledge the support from the National High Technology Research and Development Program of China (863 Program; Grant No. 2013AA031903), the youth 973 program (2015CB932700), the National Natural Science Foundation of China (Grant Nos. 51222208, 51290273, 61222505, and 61435010), the Doctoral Fund of Ministry of Education of China (Grant No. 20123201120026), ARC DECRA (DE120101569), DP (DP140101501), China Postdoctoral Science Foundation (2014M550303, 2015M572353), the Natural Science Foundation of Guangdong Province, China (2014A030310416), and Engineering Seed Funding Scheme (2014) in Monash University. This work was performed in part at the Melbourne Centre for Nanofabrication (MCN) in the Victorian Node of the Australian National Fabrication Facility (ANFF).

REFERENCES

(1) Bao, Q.; Zhang, H.; Wang, Y.; Ni, Z.; Yan, Y.; Shen, Z. X.; Loh, K. P.; Tang, D. Y. Atomic-layer graphene as a saturable absorber for ultrafast pulsed lasers. *Adv. Funct. Mater.* **2009**, *19*, 3077−3083.

(2) Bao, Q.; Loh, K. P. Graphene photonics, plasmonics, and broadband optoelectronic devices. *ACS Nano* **2012**, *6*, 3677−3694.

DOI: 10.1021/acsphotonics.5b00193
ACS Photonics 2015, 2, 832−841

(3) Keller, U. Recent developments in compact ultrafast lasers. *Nature* **2003**, *424*, 831−838.
(4) Wang, F.; Rozhin, A. G.; Scardaci, V.; Sun, Z.; Hennrich, F.; White, I. H.; Milne, W. I.; Ferrari, A. C. Wideband-tuneable, nanotube mode-locked, fibre laser. *Nat. Nanotechnol.* **2008**, *3*, 738−742.
(5) Choi, S. Y.; Cho, D. K.; Song, Y.-W.; Oh, K.; Kim, K.; Rotermund, F.; Yeom, D.-I. Graphene-filled hollow optical fiber saturable absorber for efficient soliton fiber laser mode-locking. *Opt. Express* **2012**, *20*, 5652−5657.
(6) Lin, Y.-H.; Yang, C.-Y.; Liou, J.-H.; Yu, C.-P.; Lin, G.-R. Using graphene nano-particle embedded in photonic crystal fiber for evanescent wave mode-locking of fiber laser. *Opt. Express* **2013**, *21*, 16763−16776.
(7) Zhu, G.; Zhu, X.; Balakrishnan, K.; Norwood, R. A.; Peyghambarian, N. Fe 2+: ZnSe and graphene Q-switched singly Ho^{3+}-doped ZBLAN fiber lasers at 3 μm. *Opt. Mater. Express* **2013**, *3*, 1365−1377.
(8) Bao, Q.; Zhang, H.; Ni, Z.; Wang, Y.; Polavarapu, L.; Shen, Z.; Xu, Q.-H.; Tang, D.; Loh, K. P. Monolayer graphene as a saturable absorber in a mode-locked laser. *Nano Res.* **2011**, *4*, 297−307.
(9) Sheng, Q.-W.; Feng, M.; Xin, W.; Guo, H.; Han, T.-Y.; Li, Y.-G.; Liu, Y.-G.; Gao, F.; Song, F.; Liu, Z.-B. Tunable graphene saturable absorber with cross absorption modulation for mode-locking in fiber laser. *Appl. Phys. Lett.* **2014**, *105*, 041901.
(10) Cho, W. B.; Kim, J. W.; Lee, H. W.; Bae, S.; Hong, B. H.; Choi, S. Y.; Baek, I. H.; Kim, K.; Yeom, D.-I.; Rotermund, F. High-quality, large-area monolayer graphene for efficient bulk laser mode-locking near 1.25 μm. *Opt. Lett.* **2011**, *36*, 4089−4091.
(11) Baek, I. H.; Lee, H. W.; Bae, S.; Hong, B. H.; Ahn, Y. H.; Yeom, D.-I.; Rotermund, F. Efficient mode-locking of sub-70-fs Ti: sapphire laser by graphene saturable absorber. *Appl. Phys. Express* **2012**, *5*, 032701.
(12) Feng, T.; Zhao, S.; Yang, K.; Li, G.; Li, D.; Zhao, J.; Qiao, W.; Hou, J.; Yang, Y.; He, J. Diode-pumped continuous wave tunable and graphene Q-switched Tm: LSO lasers. *Opt. Express* **2013**, *21*, 24665−24673.
(13) Mary, R.; Brown, G.; Beecher, S. J.; Torrisi, F.; Milana, S.; Popa, D.; Hasan, T.; Sun, Z.; Lidorikis, E.; Ohara, S. 1.5 GHz picosecond pulse generation from a monolithic waveguide laser with a graphene-film saturable output coupler. *Opt. Express* **2013**, *21*, 7943−7950.
(14) Martinez, A.; Sun, Z. P. Nanotube and graphene saturable absorbers for fibre lasers. *Nat. Photonics* **2013**, *7*, 842−845.
(15) Zhao, C.; Zou, Y.; Chen, Y.; Wang, Z.; Lu, S.; Zhang, H.; Wen, S.; Tang, D. Wavelength-tunable picosecond soliton fiber laser with topological insulator: Bi_2Se_3 as a mode locker. *Opt. Express* **2012**, *20*, 27888−27895.
(16) Luo, Z.; Huang, Y.; Weng, J.; Cheng, H.; Lin, Z.; Xu, B.; Cai, Z.; Xu, H. 1.06 μm Q-switched ytterbium-doped fiber laser using few-layer topological insulator Bi_2Se_3 as a saturable absorber. *Opt. Express* **2013**, *21*, 29516−29522.
(17) Tang, P.; Zhang, X.; Zhao, C.; Wang, Y.; Zhang, H.; Shen, D.; Wen, S.; Tang, D.; Fan, D. Topological insulator: Saturable absorber for the passive Q-switching operation of an in-band pumped 1645-nm Er: YAG ceramic laser. *IEEE Photonics J.* **2013**, *5*, 1500707−1500707.
(18) Chen, Y.; Wu, M.; Tang, P.; Chen, S.; Du, J.; Jiang, G.; Li, Y.; Zhao, C.; Zhang, H.; Wen, S. The formation of various multi-soliton patterns and noise-like pulse in a fiber laser passively mode-locked by a topological insulator based saturable absorber. *Laser Phys. Lett.* **2014**, *11*, 055101.
(19) Jung, M.; Lee, J.; Koo, J.; Park, J.; Song, Y.-W.; Lee, K.; Lee, S.; Lee, J. H. A femtosecond pulse fiber laser at 1935 nm using a bulk-structured Bi_2Te_3 topological insulator. *Opt. Express* **2014**, *22*, 7865−7874.
(20) Lin, Y.-H.; Yang, C.-Y.; Lin, S.-F.; Tseng, W.-H.; Bao, Q.; Wu, C.-I.; Lin, G.-R. Soliton compression of the erbium-doped fiber laser weakly started mode-locking by nanoscale p-type Bi_2Te_3 topological insulator particles. *Laser Phys. Lett.* **2014**, *11*, 055107.
(21) Sotor, J.; Sobon, G.; Macherzynski, W.; Abramski, K. Harmonically mode-locked Er-doped fiber laser based on a Sb_2Te_3 topological insulator saturable absorber. *Laser Phys. Lett.* **2014**, *11*, 055102.
(22) Sotor, J.; Sobon, G.; Macherzynski, W.; Paletko, P.; Grodecki, K.; Abramski, K. M. Mode-locking in Er-doped fiber laser based on mechanically exfoliated Sb_2Te_3 saturable absorber. *Opt. Mater. Express* **2014**, *4*, 1−6.
(23) Wang, K.; Wang, J.; Fan, J.; Lotya, M.; O'Neill, A.; Fox, D.; Feng, Y.; Zhang, X.; Jiang, B.; Zhao, Q. Ultrafast saturable absorption of two-dimensional MoS_2 nanosheets. *ACS Nano* **2013**, *7*, 9260−9267.
(24) Zhang, H.; Lu, S.; Zheng, J.; Du, J.; Wen, S.; Tang, D.; Loh, K. Molybdenum disulfide (MoS_2) as a broadband saturable absorber for ultrafast photonics. *Opt. Express* **2014**, *22*, 7249−7260.
(25) Wang, S.; Yu, H.; Zhang, H.; Wang, A.; Zhao, M.; Chen, Y.; Mei, L.; Wang, J. Broadband few-layer MoS_2 saturable absorbers. *Adv. Mater.* **2014**, *26*, 3538−3544.
(26) Chen, S. Q.; Zhao, C. J.; Li, Y.; Huang, H. H.; Lu, S. B.; Zhang, H.; Wen, S. C. Broadband optical and microwave nonlinear response in topological insulator. *Opt. Mater. Express* **2014**, *4*, 587−596.
(27) Hajlaoui, M.; Papalazarou, E.; Mauchain, J.; Lantz, G.; Moisan, N.; Boschetto, D.; Jiang, Z.; Miotkowski, I.; Chen, Y.; Taleb-Ibrahimi, A. Ultrafast surface carrier dynamics in the topological insulator Bi_2Te_3. *Nano Lett.* **2012**, *12*, 3532−3536.
(28) Wang, Y.; Hsieh, D.; Sie, E.; Steinberg, H.; Gardner, D.; Lee, Y.; Jarillo-Herrero, P.; Gedik, N. Measurement of intrinsic Dirac fermion cooling on the surface of the topological insulator Bi_2Se_3 using time-resolved and angle-resolved photoemission spectroscopy. *Phys. Rev. Lett.* **2012**, *109*, 127401.
(29) Glinka, Y. D.; Babakiray, S.; Johnson, T. A.; Bristow, A. D.; Holcomb, M. B.; Lederman, D. Ultrafast carrier dynamics in thin-films of the topological insulator Bi_2Se_3. *Appl. Phys. Lett.* **2013**, 103.
(30) Song, C.-L.; Wang, Y.-L.; Jiang, Y.-P.; Zhang, Y.; Chang, C.-Z.; Wang, L.; He, K.; Chen, X.; Jia, J.-F.; Wang, Y. Topological insulator Bi_2Se_3 thin films grown on double-layer graphene by molecular beam epitaxy. *Appl. Phys. Lett.* **2010**, *97*, 143118−143118−3.
(31) Liang, B.; Song, Z.; Wang, M.; Wang, L.; Jiang, W. Fabrication and thermoelectric properties of graphene/Bi_2Te_3 composite materials. *J. Nanomater.* **2013**, *2013*, 6.
(32) Dang, W.; Peng, H.; Li, H.; Wang, P.; Liu, Z. Epitaxial heterostructures of ultrathin topological insulator nanoplate and graphene. *Nano Lett.* **2010**, *10*, 2870−2876.
(33) Ni, Z. H.; Yu, T.; Lu, Y. H.; Wang, Y. Y.; Feng, Y. P.; Shen, Z. X. Uniaxial strain on graphene: Raman spectroscopy study and band-gap opening. *ACS Nano* **2008**, *2*, 2301−2305.
(34) Shi, Y.; Fang, W.; Zhang, K.; Zhang, W.; Li, L. J. Photoelectrical response in single-layer graphene transistors. *Small* **2009**, *5*, 2005−2011.
(35) Bos, J.; Zandbergen, H.; Lee, M.-H.; Ong, N.; Cava, R. Structures and thermoelectric properties of the infinitely adaptive series $(Bi_2)_m(Bi_2Te_3)_n$. *Phys. Rev. B* **2007**, *75*, 195203.
(36) Chen, Y.; Analytis, J.; Chu, J.-H.; Liu, Z.; Mo, S.-K.; Qi, X.-L.; Zhang, H.; Lu, D.; Dai, X.; Fang, Z. Experimental realization of a three-dimensional topological insulator, Bi_2Te_3. *Science* **2009**, *325*, 178−181.
(37) Chen, M.; Peng, J.-P.; Zhang, H.-M.; Wang, L.-L.; He, K.; Ma, X.-C.; Xue, Q.-K. Molecular beam epitaxy of bilayer Bi(111) films on topological insulator Bi_2Te_3: A scanning tunneling microscopy study. *Appl. Phys. Lett.* **2012**, *101*, 081603.
(38) Suh, J.; Fu, D.; Liu, X.; Furdyna, J. K.; Yu, K. M.; Walukiewicz, W.; Wu, J. Fermi-level stabilization in the topological insulators Bi_2Se_3 and Bi_2Te_3: Origin of the surface electron gas. *Phys. Rev. B* **2014**, *89*, 115307.
(39) Yu, Y.-J.; Zhao, Y.; Ryu, S.; Brus, L. E.; Kim, K. S.; Kim, P. Tuning the graphene work function by electric field effect. *Nano Lett.* **2009**, *9*, 3430−3434.
(40) Zhang, H.; Virally, S.; Bao, Q.; Kian Ping, L.; Massar, S.; Godbout, N.; Kockaert, P. Z-scan measurement of the nonlinear refractive index of graphene. *Opt. Lett.* **2012**, *37*, 1856−1858.

DOI: 10.1021/acsphotonics.5b00193
ACS Photonics 2015, 2, 832−841

(41) Kurtner, F.; der Au, J. A.; Keller, U. Mode-locking with slow and fast saturable absorbers-What's the difference? *IEEE J. Sel. Top. Quant.* **1998**, *4*, 159−168.
(42) George, P. A.; Strait, J.; Dawlaty, J.; Shivaraman, S.; Chandrashekhar, M.; Rana, F.; Spencer, M. G. Ultrafast optical-pump terahertz-probe spectroscopy of the carrier relaxation and recombination dynamics in epitaxial graphene. *Nano Lett.* **2008**, *8*, 4248−4251.
(43) Hong, X.; Kim, J.; Shi, S.-F.; Zhang, Y.; Jin, C.; Sun, Y.; Tongay, S.; Wu, J.; Zhang, Y.; Wang, F., Ultrafast charge transfer in atomically thin MoS_2/WS_2 heterostructures. *Nat. Nanotechnol.* **2014**, *167*.
(44) Smith, N. J.; Blow, K.; Andonovic, I. Sideband generation through perturbations to the average soliton model. *J. Lightwave Technol.* **1992**, *10*, 1329−1333.
(45) Zhang, H.; Tang, D.; Zhao, L.; Bao, Q.; Loh, K. P. Vector dissipative solitons in graphene mode locked fiber lasers. *Opt. Commun.* **2010**, *283*, 3334−3338.
(46) Keller, U.; Weingarten, K. J.; Kartner, F. X.; Kopf, D.; Braun, B.; Jung, I. D.; Fluck, R.; Honninger, C.; Matuschek, N.; Aus der Au, J. Semiconductor saturable absorber mirrors (SESAM's) for femtosecond to nanosecond pulse generation in solid-state lasers. *IEEE J. Sel. Top. Quantum Electron.* **1996**, *2*, 435−453.
(47) Li, X.; Cai, W.; An, J.; Kim, S.; Nah, J.; Yang, D.; Piner, R.; Velamakanni, A.; Jung, I.; Tutuc, E. Large-area synthesis of high-quality and uniform graphene films on copper foils. *Science* **2009**, *324*, 1312−1314.

DOI: 10.1021/acsphotonics.5b00193
ACS Photonics 2015, 2, 832−841